Mixture Condensation of Ethanol/Water and Ethanol/Siloxane in a Vertical Double Pipe

Conrad Zimmermann*, Nico Lubos, Cagatay Necati Dagli, and Stephan Kabelac

Eco-friendly mixtures may substitute pure working fluids in thermodynamic cycle processes, yet the existing calculation approaches of mixture condensation are complex due to iterative procedures and multiple input data. To simplify condenser design, this project aims for a new calculation method of mixtures. On this behalf, experimental data for the condensation of ethanol/water and ethanol/octamethyltrisiloxane is provided within a wide composition range to identify the most influential parameters. Finally, a practical prediction method for heat transfer coefficients of mixtures is suggested.

Keywords: Condensation, Heat transfer, Mixtures, Siloxane

1 Introduction

Vapor-liquid equilibria (VLE) of mixtures play an important role in the process engineering industry and the condensation of mixture vapor bears challenges in particular for the efficient apparatus design of liquefiers. Furthermore, mixed refrigerants are seen as potential working fluids in thermodynamic cycles in order to replace conventional pure hydrofluorocarbons with large global warming potential [1]. However, the behavior of mixtures during phase change is more complex in comparison to those of pure fluids and the prediction still comes with large uncertainties. At the same time, the precise design of heat exchangers is important to achieve high efficiencies.

With regard to this apparatus design, there are different approaches available for the prediction of the heat transfer coefficients (HTCs) during film condensation of mixtures, which can be categorized into (i) conservation equation, (ii) non-equilibrium, (iii) equilibrium and (iv) empirical approaches, as presented in the review article of Fronk and Garimella [2]. Sparrow and Marshall [3] establish a very theoretical and calculation intensive solution of the conservation equations, while Colburn and Drew [4] introduce an iterative calculation procedure that combines heat and mass transfer correlations based on the assumption of a non-equilibrium between vapor and condensate. On the contrary, Silver [5], Bell and Ghaly [6] assume that the vapor and condensate do exist in equilibrium, so that mass transfer is not explicitly considered. Therefore, the calculation procedure is reduced, but the physical background is less accurate. Lastly, as an example, Tandon et al. [7] develop an empirical correlation for their specific mixture and geometry, which gives quick results, but in general is not applicable to other cases. All these models refer to film conden-

sation and none of them is capable of implementing dropwise condensation due to their inherent boundary conditions. Although the non-equilibrium method represents a more sophisticated description of the condensation process, the equilibrium method can also lead to satisfying results and keeps the benefit of less computing time. Still, these approaches coexist, and different aspects and adjustments of the approaches are investigated in current literature [8, 9].

To give clear guidance in the decision of using one or another prediction method, Macdonald and Garimella [10] present criteria when to neglect mass transfer resistance, i.e., use the equilibrium approach. However, Dorao and Fernandino [11] screened a large set of experimental data and find that the prediction of heat transfer deterioration during mixture condensation can be reduced to a strong dependency on the change of thermophysical mixture properties rather than additional mixture effects such as the mass transfer resistance.

However, the development nowadays tends to focus on practical prediction approaches. This is also driven by the growing amount of experimental data, which can only be validated by models with reduced complexity of iteration and input data. Furthermore, the applicability of the theoretical approaches is very limited for different condenser geometries and boundary conditions. In this context, Del Col et al. [12] incorporate flow patterns into a model

[1]Conrad Zimmermann https://orcid.org/0000-0002-3161-0974 (zimmermann@ift.uni-hannover.de), [1]Nico Lubos, [1]Cagatay Necati Dagli, [1]Prof. Dr.-Ing. Stephan Kabelac
[1]Institute of Thermodynamics, Leibniz University Hannover, Welfengarten 1, 30167 Hannover, Germany.

based on the more practical equilibrium approach, in order to predict flow condensation of zeotropic mixtures in horizontal tubes. Zhang et al. [13] investigate condensation of R134a/R245fa in plate heat exchangers with a wide range of compositions. They find that the process is shear-controlled similar to pure fluids, but the non-isothermal condensation due to the temperature glide of a condensing mixture (cf. Fig. 2) is most influential on the heat transfer deterioration, as the driving temperature gradient decreases in the progress of condensation. They apply a modified equilibrium approach, which gives good prediction of their results. In contrast, Mazumder et al. [14], who conduct extensive experimental studies on the condensation of R32/R1234ze(E) in horizontal tubes, state that models from literature over- or underestimate their results. Hence, they develop their own prediction method for the local HTC of condensing mixtures based on a liquid film HTC combined with an extra term that allows for influential mixture parameters, such as the temperature glide.

In summary, systematic experimental data on zeotropic mixture condensation still needs to grow for comprehensive understanding and the given model approaches for the prediction of zeotropic mixture condensation need continuous revision for practical use. Therefore, this article contributes experimental data for condensation of water, ethanol and octamethyltrisiloxane (MDM) and their binary mixtures ethanol/water and ethanol/MDM within a wide range of compositions. A combination of water and MDM is not possible due to immiscibility. The goal is to provide a practical pre-design method for the industrial sector for the total condensation of mixtures that evolves from pure fluid condensation with adjustable mixture parameters.

2 Methods

2.1 Experimental Setup and Procedure

The experimental setup is a closed loop as shown in Fig. 1 consisting of a high-pressure part, where the mixture vapor is generated, and a low-pressure part including the investigation of mixture condensation. The mixture vapor is formed in an isobaric evaporator and released to the test section through a controlled needle valve. The vapor is then pre-conditioned in a helical coil heat exchanger before it enters the condenser section. This condenser section is a vertical double pipe, the inner pipe is made of stainless steel and cooled inside by a thermostat fluid, the outer pipe is a transparent polycarbonate pipe. The mixture vapor enters the annulus between the two pipes and condenses on the outside of the inner pipe. Condensate and residual vapor are separated at the bottom of the condenser section and the residual vapor is liquefied in an additional plate heat exchanger. The condensate from the measuring section flows into an inline optical measuring cell that is connected to an FTIR spectroscope via glass fiber cables to determine the composition of the condensate. Condensate from the FTIR cell and condensate from the liquefier are collected in a receiver tank and pumped back with a gear pump into the isobaric evaporator.
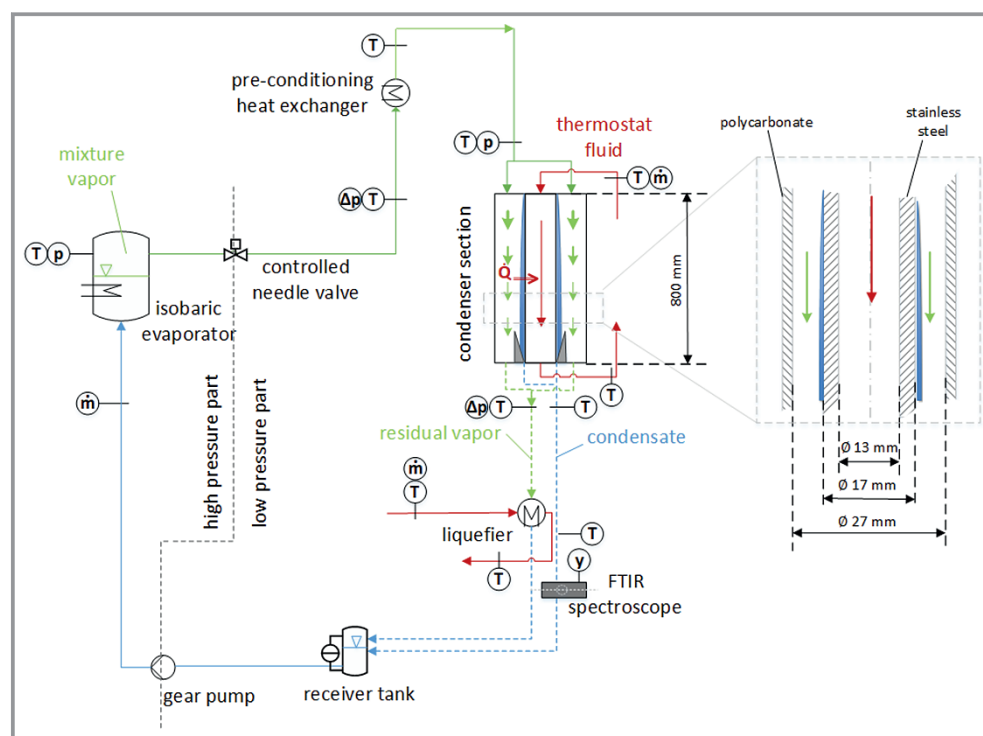

Figure 1. Simplified P&I diagram of the experimental setup with geometry of the condenser section.

The investigation comprises condensation of various compositions of both mixtures, the influence of vapor mass flow rates by different needle valve opening degrees and numerous driving temperature gradients in the condenser section. These different operating conditions lead to partial or total condensation, which shall be considered in the evaluation. Here, total condensation means that the vapor quality at the outlet of the condenser section just reached zero. Thus, it is important to precisely meet these operating points. This is achieved by a careful lowering of the thermostat temperature until two indicators of the total condensation occur: (1) the liquefier for residual vapor does not receive any heat, which is acquired by an energy balance, and (2) the temperature at the vapor outlet falls below the expected equilibrium temperature. Both observations happen exactly, when the last vapor is just liquefied in the condenser section.

In addition to that, the composition of the condensate is measured in the FTIR cell during total condensation and is then taken as the vapor composition in all mutual operating points with partial condensation. Furthermore, in operating points of partial condensation, the FTIR measurement is used to connect the condensate composition with the mode of dropwise or film condensation. In the future, the FTIR might help with further interpretation of the results. The reference curves for the FTIR measurement are recorded in advance for several different compositions with a separate setup. Further instrumentation and its positioning can be taken from Fig. 1 and the assessment of the measurement uncertainties is given in Tab. 1.

Table 1. Uncertainties of measurement instrumentation.

Parameter	Uncertainty
Temperature T [K]	± 0.1
Pressure p [mbar]	± 3
Mass flow rate $\dot{m}$ [g s^{-1}]	± 0.02
Mass fraction y [mass%]	± 0.5

As the low-pressure part of the system is below atmospheric pressure with $p_{sys} = 0.11–0.26$ bar, the vacuum tightness is checked frequently, and potential inert gas is removed with a water jet pump between two measurement points. The low system pressure results in lower saturation temperatures, which is necessary to work with the polycarbonate pipe, especially for MDM, and beneficial to reduce heat losses. During operation, the corresponding vapor mass flow rate is evaluated via the sensor downstream of the gear pump and the liquid level in the receiver tank is kept constant.

2.2 Calculation of Heat Transfer Coefficients

Primarily, the amount of heat transferred to the thermostat fluid, in this case water, is calculated by means of an energy balance, using a caloric equation of state for incompressible fluids. The total heat flow rate $\dot{Q}_{tot}$ is then

$$\dot{Q}_{tot} = \dot{m}_{tf}\bar{c}_{tf}\left(T_{tf,out} - T_{tf,in}\right) \tag{1}$$

where $\dot{m}_{tf}$ is the mass flow rate of the thermostat fluid, $\bar{c}_{tf}$ is the average specific heat capacity, and $T_{tf,in}$ and $T_{tf,out}$ are the inlet and outlet temperatures of the thermostat fluid. This total heat flow rate $\dot{Q}_{tot}$ combines mainly the heat of the condensation process itself and some sensible heat of the vapor, as the vapor enters the measurement section slightly superheated to prevent condensation upstream. To obtain the heat transfer rate of condensation $\dot{Q}_{con}$, it is assumed that heat loss is negligible due to sufficient insulation, and the sensible heat transfer rate $\dot{Q}_{sen,v}$ needs to be subtracted from the total heat. Thus, it is

$$\dot{Q}_{con} = \dot{Q}_{tot} - \dot{Q}_{sen,v} \tag{2}$$

where $\dot{Q}_{sen,v}$ is calculated by the energy balance of the vapor

$$\dot{Q}_{sen,v} = \dot{m}_v\bar{c}_{p,v}\left(T_{v,in} - T_{d,in}\right) \tag{3}$$

with $\dot{m}_v$ as the vapor mass flow rate at the inlet of the measuring section, $\bar{c}_{p,v}$ is the mean specific isobaric heat capacity of the vapor, $T_{v,in}$ is the temperature of the superheated vapor at the inlet and $T_{d,in}(p_{s,in},y_{v,in})$ is the corresponding dew point temperature to the inlet saturation pressure $p_{s,in}$ and the vapor mass fraction $y_{v,in}$. $\dot{Q}_{con}$ considers the latent heat of condensation $\dot{Q}_{lat}$ as well as the sensible heat from the subcooling of the condensate $\dot{Q}_{sen,c}$. Especially in the case of mixture condensation, $\dot{Q}_{sen,c}$ can be significant due to large temperature glides between dew point and bubble point.

The heat transfer rate of condensation $\dot{Q}_{con}$ from the energy balance in Eq. (2) can also be expressed in terms of an overall heat transfer coefficient U

$$\dot{Q}_{con} = UA_o \cdot \Delta T_{log} \tag{4}$$

with the outer surface area A_o of the stainless-steel pipe and the logarithmic temperature difference ΔT_{log}, often referred to as *LMTD*. The *LMTD* is calculated as follows for the case of vapor and thermostat fluid in co-current flow

$$\Delta T_{log} = \frac{\left(T_{d,in} - T_{tf,in}\right) - \left(T_{v,out} - T_{tf,out}\right)}{\ln\left(\frac{T_{d,in} - T_{tf,in}}{T_{v,out} - T_{tf,out}}\right)} \tag{5}$$

$T_{v,out}$ is the vapor temperature at the outlet of the condenser section for the case of partial condensation. For total condensation, $T_{v,out}$ is replaced by the temperature on the bubble line $T_{b,out}(p_{s,out},y_{v,in})$, evaluated at the outlet satura-

tion pressure $p_{s,out}$. For the case of pure fluid condensation, $T_{d,in}$ and $T_{v,out}$ are replaced by the saturation temperature of the pure substance at $T_{s,0}(p_{s,in})$ and $T_{s,0}(p_{s,out})$, respectively, independent of the vapor quality at the outlet. The overall heat transfer coefficient U is used to calculate the HTC of condensation a_{con} with Eq. (6):

$$\frac{1}{UA_o} = \frac{1}{\alpha_i A_i} + \frac{1}{2\lambda_{st}\pi L}\ln\left(\frac{A_o}{A_i}\right) + \frac{1}{\alpha_{con}A_o} \quad (6)$$

Here, a_i is the heat transfer coefficient between the thermostat fluid and the inner wall of the stainless-steel pipe with the inner surface area A_i, the thermal conductivity of steel is $\lambda_{st} = 15\,W\,m^{-1}K^{-1}$. Although the heat transfer kinetic is partly influenced by the desuperheating, visual investigation showed that the condensation starts at the very top of the condenser section, so that the total length of the steel pipe is considered to contribute to the effective condensing area for the calculation of α_{con}. The inner HTC α_i can be calculated from the Nusselt correlation for fully developed turbulent internal flows of Gnielinski [15]. Laminar film condensation of pure fluids is calculated with Nusselt's film theory for mean heat transfer coefficients.

The thermophysical properties of all fluids come from REFPROP 10.0, missing data for MDM is obtained from ChemCAD. Essential data of pure fluids is listed in Tab. 2. It is assumed that the uncertainties of thermophysical data and, equally, of all geometrical quantities are negligible. The VLE of the mixtures are shown in Fig. 2 and taken from ChemCAD with NRTL for ethanol/water and with UNIFAC
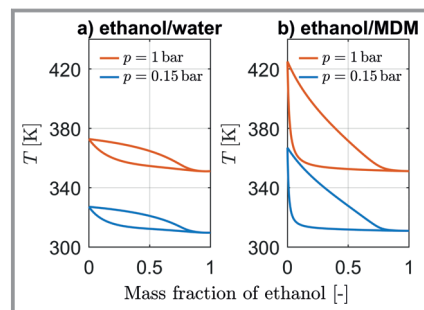

Figure 2. Phase diagrams of ethanol/water and ethanol/MDM.

Table 2. Thermophysical properties of pure fluids.

Property at 20 °C and 1 bar	Water (deionized)	Ethanol (>99.8 % purity)	MDM (>97.0 % purity)
λ_l [W m^{-1}K^{-1}]	0.598	0.164	0.132
η_l [10^{-3} kg m^{-1}s^{-1}]	1.002	1.194	0.887
ρ_l [kg m^{-3}]	998	789	820
h_{vl} (1 bar) [10^3 J kg^{-1}]	2257	850	153
$c_{p,l}$ [J kg^{-1}K^{-1}]	4184	2396	1483
σ_l [10^{-3} N m^{-1}]	73.8	22.5	17.1

for ethanol/MDM. The lower pressure of 0.15 bar corresponds to the typical mean operating pressure of the experiments.

The resulting uncertainty of the condensation HTCs is determined by using the Gaussian error propagation for all quantities and measured values. All data points in the following sections share a mean relative measurement uncertainty of less than 15 %.

3 Results and Discussion

3.1 Experimental Results of Pure Fluids

As the goal of the overall project is to develop a practical prediction method for the mixture condensation derived from pure fluid condensation, precise evaluation of the pure fluid condensation is inevitable. Fig. 3 shows the condensation HTCs measured for all three pure fluids over the *LMTD* with different vapor mass flow rates. The filled markers indicate measurement points with total condensation. The results of pure water are comprised with trend lines for a better comprehension, yet no further physical input is given with this function. However, for ethanol and MDM, the calculated results of Nusselt's film theory are added as a reference. It is reasonable to state that there is laminar film condensation in all operating points for ethanol and MDM, as they show very high accordance with Nusselt's skin theory and the Reynolds numbers of the condensate film at the outlet are smaller than 65. In comparison, the results of water show the typical behavior of dropwise condensation, which can also be observed by visual investigation. They are qualitatively similar to those of Li [16], who investigated dropwise condensation of water and ethanol/water mixtures.

3.2 Experimental Results of Ethanol/Water

Fig. 4 shows the experimental results for the mixture condensation HTCs of ethanol/water with a wide range of compositions as well as the same pure fluid results from Fig. 3.

All mass fractions given in the following section belong to the mass fraction of ethanol and relate to the vapor inlet. Different mass flow rates are investigated for each composition. Starting from low mass fractions of ethanol, it can be seen that the HTCs for a mass fraction of 12 % ethanol clearly drop to the half of pure water, while the behavior of dropwise condensation remains. For an increasing mass fraction of ethanol, this qualitative behavior slightly changes, and the minimum HTCs are reached with 61 mass% of ethanol. Then, with 76 mass% of ethanol, larger HTCs can be observed back again. Finally, at 95 mass% of ethanol and pure ethanol, the
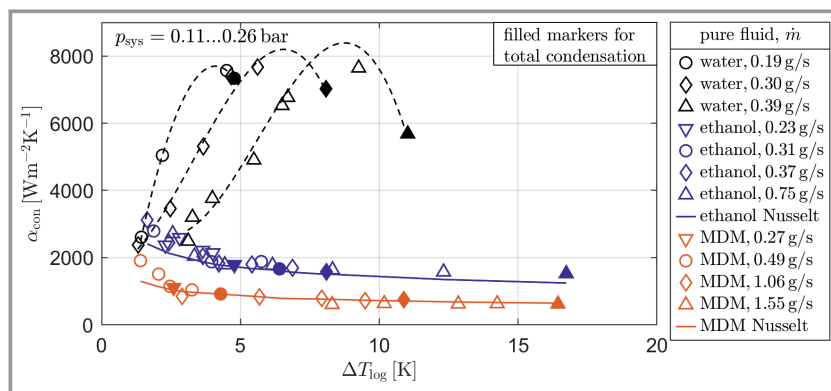
Figure 3. Pure fluid condensation HTCs with trend lines and Nusselt's laminar film condensation.
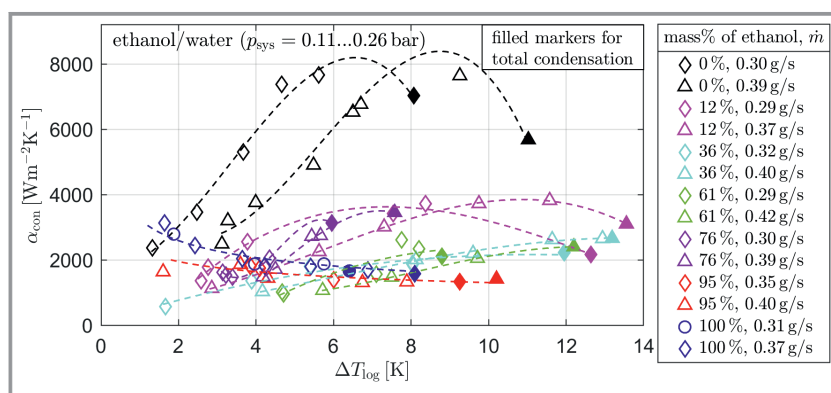

Figure 4. Mixture condensation HTCs of ethanol/water with trend lines.

characteristic of dropwise condensation switches to laminar film condensation and the HTCs are on a lower level than with all other compositions.

In order to get a better overview, the data is reduced to total condensation and plotted against the mass fraction of ethanol in Fig. 5. The figure confirms the trend of decreasing HTCs for increasing fractions of ethanol and a local maximum at 76 mass% of ethanol. This overall behavior results from a combination of different aspects, such as the change of thermophysical properties with increasing ethanol fraction, the temperature glide of the mixture, which
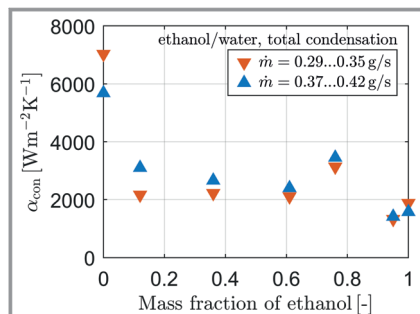

Figure 5. Total condensation HTCs of ethanol/water depending on the mass fraction of ethanol.

increases with small ethanol amounts and then decreases back again, and the condensation mode.

The most influential thermophysical properties in the context of condensation are the thermal conductivity and the heat of vaporization, which are given in Tab. 2 for pure fluids. Yet, these properties also decline monotonically when adding ethanol to water. This reveals that increasing the mass fraction of ethanol results in a smaller heat transfer capability due to the distinctly smaller values of ethanol than water. Moreover, the increasing temperature glide, as shown in Fig. 2, is another reason for the heat transfer deterioration, especially with ethanol mass fractions of 36 mass% and 61 mass%. This effect is largely discussed in literature [10, 12–14]. Mainly, the temperature glide between dew and bubble point temperature limits the condensation rate, as the wall temperature needs to be below the boiling point for total condensation. Therefore, a mixture with exactly the same properties as a pure fluid, yet with a certain temperature glide, will always have a larger driving temperature gradient $\Delta T_{\log}$ for the same heat flow rate $\dot{Q}_{\text{con}}$ with regard to Eq. (4), which finally reduces the resulting mixture condensation HTC.

Physically, the composition of the vapor and thus its saturation temperature decreases during the condensation, so that sensible heat of the vapor and condensate film needs to be removed, which decelerates the condensation process. Beyond that, the entire behavior of ethanol/water mixture condensation is superposed by the change of the condensation mode from dropwise to laminar film condensation, as indicated in Fig. 4. In case of 76 mass% of ethanol, the temperature glide is small with less than 3 K and the condensate flow is not completely laminar, but has wavy rivulet structures, which results in a local maximum of the HTC. In comparison, the azeotropic mixture with 95 mass% of ethanol does not have a limiting temperature glide, however the laminar film condensation is fully developed, which reduces the kinetics.

A visual observation of the condensation mode can be seen in Fig. 6. All photos are taken in the lower third of the condenser section and the given ethanol mass fractions are measured at the outlet with the FTIR. The first row of photos shows different operating points with partial condensation and indicates a detailed transition from dropwise condensation with low ethanol mass fractions to first rivulets at 7 mass%. The rivulet flow becomes dominant with increasing ethanol fraction up to 32 mass%. The second row of
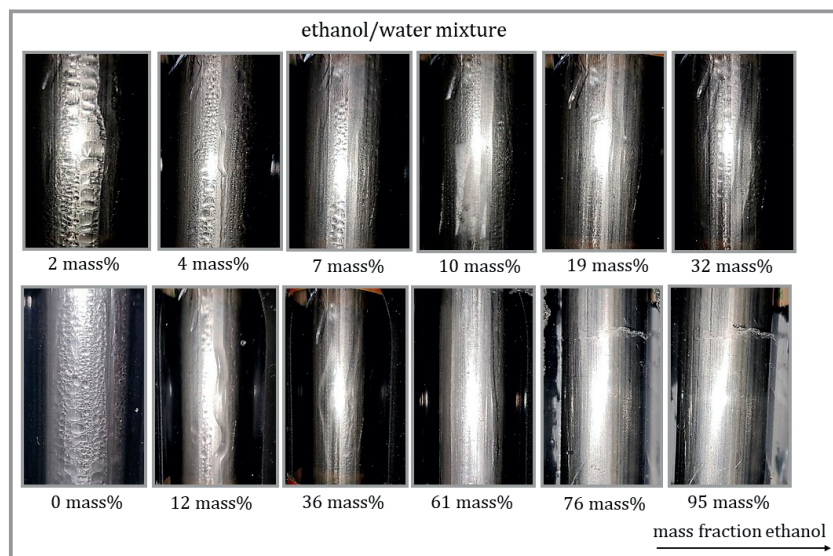
Figure 6. Condensation modes in dependence of the ethanol mass fraction

photos gives an overview of all operating points with total condensation corresponding to Fig. 5. With 61 mass% of ethanol, the rivulets are fading into film-wise condensation, yet vertical wavy structures on the surface of the condensate can still be seen up to 76 mass%. In summary, the additional complexity of the condensation modes of ethanol/water makes it hard to distinguish between the proportional influence of the different mixture effects mentioned above. Hence, this fluid combination is not suitable for the development of a new prediction method, where such boundary conditions should be kept constant. Consequently, the second fluid combination is chosen as ethanol and MDM, as both of them and also their mixtures show laminar film condensation.

3.3 Experimental Results of Ethanol/MDM

Analog to the investigation of ethanol/water, the experimental results for mixture condensation of ethanol/MDM are presented in Fig. 7. Proceeding from pure MDM, there is already a substantial drop of the mixture HTC for a very small ethanol fraction of 0.7 mass% and the HTC further decrease for increasing ethanol fractions up to 45 mass%. In general, this heat transfer deterioration needs to be associated with the condensation process through the vapor-liquid region, often referred to as the mass transfer resistance, rather than the change of thermophysical properties. The distinctly increased amount of ethanol still leads to a strong heat transfer deterioration,

although the larger heat of vaporization and thermal conductivity of ethanol would actually be beneficial to the HTC. Furthermore, the shape of the graphs are typical for laminar film condensation, yet this shape changes with 21 mass% ethanol, where the HTCs increase slightly with $LMTD > 15$ K. This trend increases and is dominant for ethanol mass fractions of 71 mass% and 84 mass%. Here, the behavior is not a result of partial dropwise condensation, as laminar film condensation can be observed in all operating points for this mixture and is thus not shown in a further figure. Instead, the behavior is caused by the relationship of decreasing vapor quality during the condensation process and the change of the corresponding condensate composition in combination with the temperature glide, all of which can be taken from the phase diagram in Fig. 2.

The results of total condensation for ethanol/MDM are plotted against the composition in Fig. 8. In total, Fig. 8 illustrates the shape of the mixture condensation heat transfer and underlines the drastic heat transfer deterioration, which already appears for very small amounts of ethanol in the mixture vapor. This is mainly caused by the large necessary temperature glide for total condensation and prevails up to 21 mass% of ethanol, where the HTCs begin to increase slightly, as discussed for Fig. 7. Furthermore, the pure fluid data points in Fig. 8 show decreasing HTC with higher mass flow rates, as expected from the increased thickness of the condensate film. In the case of mixtures, this relationship turns around because the heat transfer is not primarily governed by heat conduction through the condensate anymore but is also affected by the sensible subcooling of the
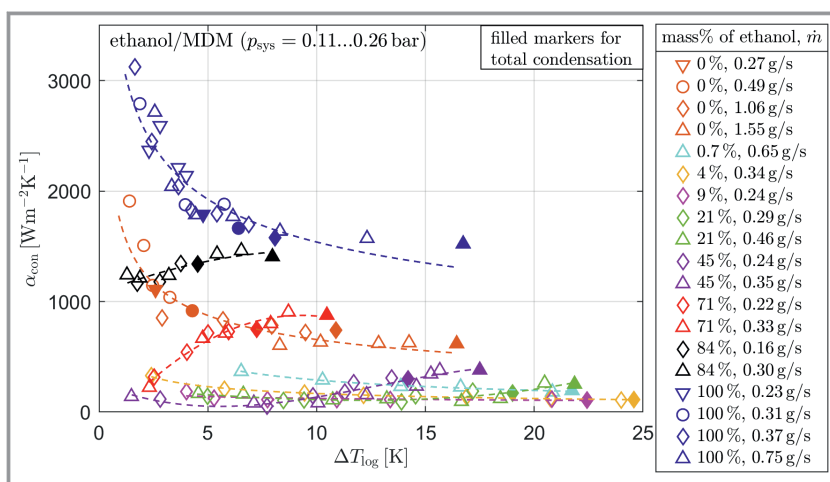

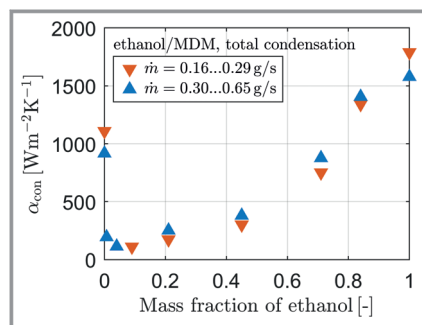**Figure 7.** HTCs of the mixture condensation with trend lines.

Figure 8. Total condensation HTCs of ethanol/MDM depending on the mass fraction of ethanol.

condensate and vapor. Hence, the larger *LMTD*, which is needed for total condensation of higher vapor mass flow rates, also results in a stronger subcooling of the condensate film, so that the condensation rate of further light component slightly amplifies and leads to larger HTCs. Still, the influence of mass flow rate is subordinate in the case laminar film condensation.

4 Conclusion and Prospect

Essentially, there are different existing prediction approaches, as presented in Sect. 1, which try to describe the mixture condensation HTCs in Fig. 7. Yet, from a mathematical point of view, the different graphs in Fig. 7 hardly share similar functional behavior. As a consequence, the complexity of the calculation and the number of potential necessary parameters for the description will be large and not very practical. Nevertheless, a rigorous prediction method for mean total condensation HTC should be developed for the pre-design of condensers using the results shown in Fig. 8. Therefore, a suggestion of a new prediction method is sketched in the following based on a superposition approach, which calculates total condensation HTCs of mixtures derived from the pure fluid HTCs. The approach is shown in Eq. (7) and is divided into a heavy component (HC) and light component (LC) part.

$$
\begin{aligned}
\alpha_{\mathrm{con}} = {}& y \cdot \alpha_{\mathrm{con,LC,0}} \cdot \exp\left(-a_{\mathrm{LC}}(1-y)^{b_{\mathrm{LC}}}\right) \\
& + (1-y) \cdot \alpha_{\mathrm{con,HC,0}} \cdot \exp\left(-a_{\mathrm{HC}} \cdot y^{b_{\mathrm{HC}}}\right)
\end{aligned}
\tag{7}
$$

The pure fluid HTCs $a_{\mathrm{con,LC/HC,0}}$ are weighted with the mass fraction of the light component y and an exponential term is used to describe the heat transfer deterioration of the mixture. The dimensionless adjustable parameters a_{LC}, a_{HC}, b_{LC} and b_{HC} in the exponential term are specific to the mixture and allow for different mixture effects such as the mass transfer resistance and the continuous change of thermophysical properties during mixture condensation due to the passing through the VLE. These parameters are calculated from experimental HTCs and need the same boundary conditions as the pure fluid HTCs in Eq. (7), such as the

same subcooling and total condensation. Fig. 9 shows the calculated HTC results of the superposition approach at a subcooling of $\Delta T_{\mathrm{sub}} = T_{\mathrm{b}} - T_{\mathrm{w}} = 3\,\mathrm{K}$ with adjustable parameters derived from the experimental results shown before.
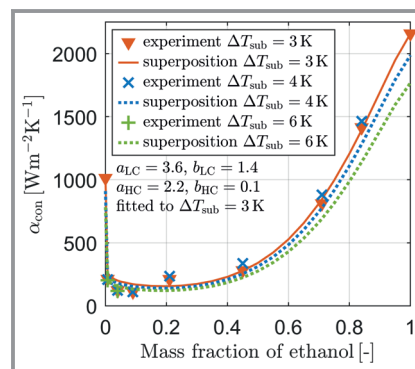

Figure 9. Comparison of experimental results with superposition approach.

The superposition approach shows good agreement with the measured HTCs. Initially, the superposition approach was developed in comparison with calculated HTC results of an equilibrium approach model, which could be reproduced with less than 10 % mean deviation by the superposition approach. Practically, the fitting of the adjustable parameters can always lead to sufficient accordance, which underlines its high functional flexibility. However, the equilibrium approach itself is not self-sufficient, but needs further adjustments with experimental values, as stated by Mazumder et al. [14]. Therefore, the superposition approach is directly compared to experimental results. The most important benefit of the superposition approach, however, is that HTCs for total condensation of any other composition or subcooling can be calculated much faster than with the existing prediction methods from literature due to an explicit correlation and without the need of extensive thermophysical mixture data. Further results of the superposition approach are calculated for $\Delta T_{\mathrm{sub}} = 4\,\mathrm{K}$ and $6\,\mathrm{K}$ with the same adjustable parameters of $\Delta T_{\mathrm{sub}} = 3\,\mathrm{K}$. The superposition approach shows good agreement with the low HTCs from the heat transfer deterioration, but larger deviations for high mass fractions of ethanol. A temperature dependence of the parameter b_{LC} could adjust this behavior, which will be part of future investigations including experiments with further mixtures and comparison to existing model approaches from literature. These new mixtures will deepen the understanding of the adjustable parameters and enable a possible generalization of them. Thus, a pre-calculation of the parameters only with pure fluid properties and VLE data of the mixture could hopefully be possible, reducing the number of validation experiments significantly.

Acknowledgment

Symbols used

A	[m²]	Surface area
$\bar{c}_{tf}$	[J kg⁻¹K⁻¹]	Mean specific heat capacity of thermostat fluid
$\bar{c}_{p,v}$	[J kg⁻¹K⁻¹]	Mean isobaric specific heat capacity of superheated vapor
d	[m]	Diameter
g	[m s⁻²]	Gravity
h	[J kg⁻¹]	Specific enthalpy
L	[m]	Length
$\dot{m}$	[kg s⁻¹]	Mass flow rate
p	[bar]	Pressure
$\dot{Q}$	[W]	Heat flow rate
T	[K]	Temperature
ΔT_{log}	[K]	Logarithmic mean temperature difference
U	[W m⁻²K⁻¹]	Overall heat transfer coefficient
y	[kg kg⁻¹]	Mass fraction

Greek letters

α	[W m⁻²K⁻¹]	Heat tranfer coefficient
η	[Pa s]	Dynamic viscosity
λ	[W m⁻¹K⁻¹]	Thermal conductivity
ρ	[kg m⁻³]	Density
σ	[N m⁻¹]	Surface tension

Sub- and Superscripts

0	Pure substance
b	Bubble line
c	Condensate
con	Condensation
d	Dew line
i	Inner
in	Inlet
l	Liquid
log	Logarithmic
o	Outer
out	Outlet
p	Isobaric
s	Saturated
sen	Sensible
st	Stainless steel
sub	Subcooled
sys	System
tf	Thermostat fluid
tot	Total
v	Vapor
vl	Vaporization
w	Wall

Abbreviations

FTIR	Fourier transform infrared
HC	Heavy component
HTC	Heat transfer coefficient
LC	Light component
LMTD	Logarithmic mean temperature difference
MDM	Octamethyltrisiloxane
VLE	Vapor-liquid equilibrium

References

[1] K. Harby, *Renewable Sustainable Energy Rev.* **2017**, *73*, 1247–1264. DOI: https://doi.org/10.1016/j.rser.2017.02.039

[2] B. M. Fronk, S. Garimella, *Int. J. Refrig.* **2013**, *36*, 534–561.

[3] E. M. Sparrow, E. Marschall, *J. Heat Transfer* **1969**, *91*, 205–211.

[4] A. P. Colburn, T. B. Drew, *AIChE J.* **1937**, *39*, 197–212.

[5] L. Silver, *Chem. Eng.* **1947**, 380–386.

[6] K. J. Bell, M. A. Ghaly, *J. Heat Transfer* **1973**, *131 (69)*, 72–79.

[7] T. N. Tandon, H. K. Varma, C. P. Gupta, *Int. J. Refrig.* **1986**, *9*, 134–136.

[8] C. Zimmermann, C. N. Dagli, Z. Arnautovic, S. Kabelac, *J. Heat Transfer* **2021**, *143*, 09453. DOI: https://doi.org/10.1115/1.4051673

[9] B. Zhang, H. Liu, J. Dong, S. Liu, *IOP Conf. Ser.: Earth Environ. Sci.* **2019**, *277*, 042048. DOI: https://doi.org/10.1088/1755-1315/227/4/042048

[10] M. Macdonald, S. Garimella, *J. Heat Transfer* **2016**, *138*, 091502. DOI: https://doi.org/10.1115/1.4033352

[11] C. A. Dorao, M. Fernandino, *Appl. Phys. Lett.* **2019**, *114*, 171902. DOI: https://doi.org/10.1063/1.5086738

[12] D. Del Col, A. Cavallini, J. R. Thome, *J. Heat Transfer* **2005**, *127*, 221–230. DOI: https://doi.org/10.1115/1.1857951

[13] J. Zhang, B. Elmegaard, F. Haglind, *Int. J. Heat Mass Transfer* **2021**, *164*, 120577. DOI: https://doi.org/10.1016/j.ijheatmasstransfer.2020.120577

[14] S. Mazumder, H. M. M. Afroz, M. A. Hossain, A. Miyara, S. Talukdar, *Int. J. Heat Mass Transfer* **2021**, *169*, 120859.

[15] V. Gnielinski, *AIChE J.* **1976**, *16 (2)*, 359–368.

[16] Y. Li, J. Yan, L. Qiao, S. Hu, *J. Thermophys. Heat Transfer* **2008**, *22 (2)*, 247–253. DOI: https://doi.org/10.2514/1.28083